Research Article

For reprint orders, please contact reprints@future-science.com

Future Medicinal Chemistry

MC1568 inhibits HDAC6/8 activity and influenza A virus replication in lung epithelial cells: role of Hsp90 acetylation

Aim: Histone deacetylases (HDACs) regulate the life-cycle of several viruses. We investigated the ability of different HDAC-inhibitors, to interfere with influenza virus A/Puerto Rico/8/34/H1N1 (PR8 virus) replication in Madin-Darby canine kidney and NCI cells. **Results:** 3-(5-(3-Fluorophenyl)-3-oxoprop-1-en-1-yl)-1-methyl-1*H*-pyrrol-2-yl)-*N*-hydroxyacrylamide (MC1568) inhibited HDAC6/8 activity and PR8 virus replication, with decreased expression of viral proteins and their mRNAs. Such an effect may be related to a decrease in intranuclear content of viral polymerases and, in turn, to an early acetylation of Heat shock protein 90 (Hsp90), a major player in their nuclear import. Later, the virus itself induced Hsp90 acetylation, suggesting a differential and time-dependent role of acetylated proteins in virus replication. **Conclusion:** The inhibition of HDAC6/8 activity during early steps of PR8 virus replication could lead to novel anti-influenza strategy.

First draft submitted: 4 April 2016; Accepted for publication: 18 August 2016; Published online: 14 October 2016

Keywords: antiviral agents • HDACs • HDAC inhibitors • Hsp90 • influenza A virus • lysine acetylation

Simona Panella[1], Maria Elena Marcocci[2], Ignacio Celestino[1], Sergio Valente[3], Clemens Zwergel[3], Domenica Donatella Li Puma[4], Lucia Nencioni[2], Antonello Mai[5], Anna Teresa Palamara*[1,6] & Giovanna Simonetti[2]

[1]San Raffaele Pisana Scientific Institute for Research, Hospitalization & Health Care, Telematic University, 00163 Rome, Italy

[2]Department of Public Health & Infectious Diseases, 'Sapienza' University of Rome, P.le A. Moro 5, 00185 Rome, Italy

[3]Department of Drug Chemistry & Technologies, 'Sapienza' University of Rome, P.le A. Moro 5, 00185 Rome, Italy

[4]Institute of Human Physiology, Medical School, Università Cattolica, 00168 Rome, Italy

[5]Department of Drug Chemistry & Technologies, Istituto Pasteur Italia-Fondazione Cenci Bolognetti, 'Sapienza' University of Rome, P.le A. Moro 5, 00185 Rome, Italy

[6]Department of Public Health & Infectious Diseases, Istituto Pasteur Italia-Fondazione Cenci Bolognetti, 'Sapienza' University of Rome, P.le A. Moro 5, 00185 Rome, Italy

*Author for correspondence:
Tel.: +39 064 969 4310–4311
Fax: +39 064 468 625
annateresa.palamara@uniroma1.it

Every year, influenza epidemic causes numerous deaths and millions of hospitalizations, with the most frightening effects occurring when new viral strains emerge from different species. Influenza A virus (IAV) is an enveloped, negative-strand RNA virus belonging to the *Orthomyxoviridae* family. The genome of influenza A viruses is composed of eight negative-sense single-stranded RNA gene segments that encode 16 proteins [1]. IAV enters into the cell by endocytosis. Replication of the influenza virus genome occurs in the nucleus by a virally encoded heterotrimeric RNA-dependent RNA polymerase composed of PB1, PB2 and PA proteins. Each newly synthesized vRNA segment is coated with the viral nucleoprotein (NP) and the heterotrimeric polymerase complex associates with each vRNA segment. This resultant vRNP complex is exported from the nucleus and travels to the plasma membrane to be assembled with other viral proteins. Finally, budding takes place at the apical surface and new viral particles are released from the infected cells [2].

Currently, matrix protein 2 (M2) and neuroaminidase inhibitors are used to prevent and treat influenza infection. While several neuroaminidase inhibitors have been developed for the treatment of influenza, these have shown a limited window for treatment initiation, and resistant variants have been detected in the population. The older class of anti-influenza drugs, the M2 inhibitors adamantanes are no longer recommended for treatment due to their toxicity and widespread resistance [3]. The development of new anti-influenza drugs with good bioavailability and efficacy against a broad spectrum of influenza viruses, including the resistant strains, is hence strongly needed. Influenza viruses take advantage of cellular signaling pathways to

FUTURE SCIENCE part of fsg

support their life-cycle. Thus, inhibition of intracellular pathways, exploited by virus for its replication, could increase the effectiveness toward different strains and decrease the emergence of drug resistance [4–7].

The reversible lysine acetylation is now recognized as a post-translational modification that controls the activity and localization of many proteins [8]. The acetylation status of histone and nonhistone proteins is regulated by the coordinate actions of histone acetyltransferases and histone deacetylases (HDACs). HDACs are divided into four classes. Class I, comprising HDAC1–3 and HDAC8, is mainly localized in the nucleus of the cells [9]. Class II HDACs is further subdivided into class IIa (HDAC4, HDAC5, HDAC7 and HDAC9), typically resident in cytoplasm with a wide range of biological activities [9,10] and class IIb, including HDAC6 and HDAC10, localized both in nucleus and in cytoplasm [11,12]. Class III includes sirtuin 1–7 and, finally, class IV, which actually contains the sole HDAC11, whose role in human physiology and pathology is still poorly understood. The enzymatic activity of HDACs plays a pivotal role not only in cancer, but also in infectious diseases [13] and in antimicrobial responses [14].

It has been demonstrated that HDACs modulated latency in certain viruses such as HIV and HSV [15,16] through the interaction with host cell target proteins. With regard to influenza, HDACs play a role in different stages of infection, facilitating or inhibiting viral replication. In particular, at early steps of IAV infection, HDAC1, on one side, and HDAC3 and HDAC8, on the other side, display opposite effects in the entry of IAV into host cells, leading to either suppression (HDAC1) or promotion (HDAC3 and HDAC8) of viral replication [17]. HDAC8 depletion by siRNA reduced internalization by endocytosis, decreased endosome acidification and inhibited import of vRNP into the nucleus, thus leading to reduction of IAV infectivity [17]. HDAC6 plays a more complex role since it facilitates early steps of infections, while it is detrimental at late steps, by interfering with the release of new viral particles. In fact, at early steps of infection HDAC6 plays a critical role for viral uncoating and vRNP import processes through its ubiquitin zinc finger (BUZ) domain [18]. On the contrary, in late steps of infection HDAC6 is cleaved by IAV-induced caspase 3 with the removal of the BUZ domain [19] and its deacetylase activity is downregulated, leading to microtubules hyperacetylation that, in turn, increases the trafficking of viral components to plasma membrane and viral release [20,21].

On these bases, and pursuing our studies on antimicrobial activity of HDAC inhibitors (HDACis) [13,22,23], we decided to investigate the anti-influenza activity of compounds with different selectivity for the various deacetylase isoforms, by evaluating their ability to inhibit the replication of influenza virus A/Puerto Rico/8/34/H1N1 (PR8 virus) in both Madin-Darby canine kidney (MDCK) and human airway epithelial cells (NCI-H292). In particular, we checked the activity of the following inhibitors: the pan-HDAC inhibitor MC2189; the class I-selective MS-275; the class II-selective MC1568. This last compound, initially identified as a specific class IIa HDACi [24], has then been described as an inhibitor of class II (a+b) HDACs [25–37]. Here we found that MC1568 is able to inhibit at low micromolar levels, HDAC6 and 8 activity and to significantly decrease PR8 virus replication in both cell lines. In addition, treatment with MC1568 reduced the intranuclear content of viral polymerases, viral protein expression and increased the acetylation status of Hsp90, a molecular chaperone protein, that is a substrate of HDAC6 and regulates the assembly and nuclear import of influenza virus RNA polymerases [38,39].

Material & methods

Chemical

Design & synthesis of HDACi compound

Melting points were determined on a Buchi 530 melting point apparatus and are uncorrected. ^{1}H NMR and ^{13}C NMR spectra were recorded at 400 MHz and 100 MHz, respectively, on a Bruker AC 400 spectrometer; chemical shifts are reported in δ (ppm) units relative to the internal reference tetramethylsilane (Me_4Si). EIMS spectra were recorded with a Fisons Trio 1000 spectrometer; only molecular ions (M^+) and base peaks are given. All compounds were routinely checked by TLC, ^{1}H NMR and ^{13}C NMR spectra. TLC was performed on aluminium-backed silica gel plates (Merck DC, Alufolien Kieselgel 60 F254) with spots visualized by UV light. All solvents were reagent grade and, when necessary, were purified and dried by standard methods. Concentration of solutions after reactions and extractions involved the use of a rotary evaporator operating at reduced pressure of ca. 20 Torr. Organic solutions were dried over anhydrous sodium sulfate. Elemental analysis has been used to determine purity of the described compounds, that is >95%. Analytical results are within ± 0.40% of the theoretical values. All chemicals were purchased from Aldrich Chimica, Milan (Italy), or from Alfa Aesar, Milan (Italy), and were of the highest purity.

Procedure for the synthesis of the 4-(2-norbornylamino)-3-fluoroacetophenone **(1)**

A suspension of 3,4-difluoroacetophenone (9.6 mmol, 1.2 ml), dry potassium carbonate (38.42 mmol, 5.31 g) and 2-aminonorbornane hydrochloride (48 mmol, 7.0 g) in dry *N,N*-dimethylformamide (DMF) (20 ml) was stirred at 90°C overnight. The reaction was quenched with water (50 ml) and extracted with diethyl ether (3 × 30 ml), the

organic phases were washed with brine (3 × 30 ml), dried with sodium sulfate and concentrated to provide an oily residue that was chromatographed on silica gel 60 eluting with ethyl acetate/*n*-hexane 1/5 to afford the pure product 1 [22]. as a yellow oil; Yield: 59%. ^{1}H NMR ($CDCl_3$) δ 1.17–1.29 (m, 4H, norbornyl protons), 1.42–1.54 (m, 3H, norbornyl protons), 1.87–1.92 (m, 1H, norbornyl proton), 2.28–2.32 (m, 2H, norbornyl protons), 2.47 (s, 3H, C*H*$_3$), 3.27–3.32 (m, 1H, norbornyl protons), 4.27 (bs, 1H, N*H*), 6.56–6.60 (t, 1H, benzene proton), 7.54–7.58 (d, 1H, benzene proton), 7.62–7.64 (d, 1H, benzene proton) ppm; ^{13}C-NMR (100 MHz, $CDCl_3$) δ 26.6, 28.0, 29.2, 35.7, 36.8, 40.2, 41.5, 58.2, 114.4, 115.1, 125.3, 126.7, 134.8, 154.6, 197.1 ppm; MS (EI): *m*/*z*: 247.14 $(M)^+$.

Procedure for the synthesis of Ethyl 3-(5-formyl-1-methyl-1*H*-pyrrol-2-yl)-2-propenoate **(2)**

A 20 ml dichloromethane solution of oxalyl chloride (0.06 mol, 5.2 ml) was added to a cooled (0°C) solution of *N,N*-dimethylformamide (0.06 mol, 4.6 ml) in dichloromethane (20 ml) over a period of 10 min. After being stirred at room temperature (RT) for 15 min, the suspension was again cooled (0°C) and treated with a solution of ethyl 3-(1-methyl-1*H*-pyrrol-2-yl)-2-propenoate (0.06 mol, 10.7 g) in dichloromethane (20 ml) [23]. The mixture was stirred at RT room temperature for 1 h and then was poured onto crushed ice (100 g) containing 2N NaOH (50 ml) and stirred for 10 min. The organic layer was separated, and the aqueous one was extracted with dichloromethane (3 × 30 ml). The combined organic solutions were washed with brine, dried and evaporated to dryness. The residual solid was purified by recrystallization (cyclohexane) to afford the pure compound 2. Melting point: 102–104°C; Yield: 78%; ^{1}H NMR ($CDCl_3$) δ1.33–1.37 (t, 3H, $COOCH_2CH_3$), 4.06 (s, 3 H, NCH_3), 4.26–4.30 (q, 2H, $COOCH_2CH_3$), 6.41–6.45 (d, 1H, CH = C*H*COOEt), 6.67–6.68 (d, 1H, pyrrole H-3 proton), 6.94–6.95 (d, 1H, pyrrole H-4 proton), 7.62–7.66 (d, 1H, C*H* = CHCOOEt), 9.61 (s, 1H, C*H*O) ppm; ^{13}C NMR ($CDCl_3$) δ 14.3, 37.6, 60.6, 115.8, 118.6, 122.9, 129.9, 130.2, 136.8, 167.8, 181.9 ppm; MS (EI): *m*/*z*: 207.09 $(M)^+$.

Procedure for the synthesis of (E)-ethyl 3-(5-((E)-3-(4-(2-norbornylamino)-3-fluorophenyl)-3-oxoprop-1-enyl)-1-methyl-1H-pyrrol-2-yl)acrylate (3) and (E)-ethyl 3-(5-((E)-3-(3-fluorophenyl)-3-oxoprop-1-enyl)-1-methyl-1H-pyrrol-2-yl)acrylate (4). Example: synthesis of (E)-ethyl 3-(5-((E)-3-(3-fluorophenyl)-3-oxoprop-1-enyl)-1-methyl-1H-pyrrol-2-yl)acrylate (4)

To a solution of sodium ethoxyde (2.3 mmol, 0.053 g Na) in ethanol (20 ml), 3-fluoroacetophenone (1.92 mmol, 0.24 ml) and (E)-ethyl 3-(5-formyl-1-methyl-1H-pyrrol-2-yl)acrylate 2 (1.92 mmol, 0.40 g) were added at 0°C, and the resulting mixture was stirred at room temperature (RT) for 5 h. The precipitate was filtered, washed first with a few drops of ethanol, then with petroleum ether (3 × 10 ml) to obtain compound 4 as a yellow solid that was recrystallized by acetonitrile; melting point: 173–175°C; yield: 78%; ^{1}H-NMR ($CDCl_3$) δ 1.29–1.33 (m, 3H, $COOCH_2CH_3$), 3.75 (s, 3H, NCH_3), 4.21–4.25 (m, 2H, $COOCH_2CH_3$), 6.22–6.26 (d, 1H, CH = C*H*COOEt), 6.61–6.65 (t, 1H, benzene proton), 6.71–6.72 (d, 1H, pyrrole H-3 proton), 6.81–6.82 (d, 1H, pyrrole H-4 proton), 7.33–7.36 (d, 1H, PhCOC*H* = CH), 7.58–7.62 (m, 1H, C*H* = CHCOOEt), 7.66–7.78 (m, 4H, PhCOCH = C*H* and benzene protons) ppm; ^{13}C NMR ($CDCl_3$) δ 14.3, 37.8, 60.6, 115.8,116.1, 117.7, 117.9 (2C), 119.0, 125.3, 125.4, 129.9, 130.3, 131.1 (2C), 137.4, 163.2, 167.8, 190.9 ppm; MS (EI): *m*/*z*: 327.13 $(M)^+$.

(E)-ethyl-3-(5-((E)-3-(4-(2-norbornylamino)-3-fluorophenyl)-3-oxoprop-1-enyl)-1-methyl-1H-pyrrol-2-yl)acrylate **(3)**

Recrystallized by benzene/acetonitrile; melting point: 168–170°C; yield: 67.9%; ^{1}H-NMR ($CDCl_3$) δ 1.17–1.33 (m, 7H, $COOCH_2CH_3$ and norbornyl protons), 1.42–1.54 (m, 3H, norbornyl protons), 1.87–1.92 (m, 1H, norbornyl proton), 2.28–2.32 (m, 2H, norbornyl protons), 3.27–3.32 (m, 1H, norbornyl protons), 3.75 (s, 3H, NCH_3), 4.22–4.24 (m, 2H, $COOCH_2CH_3$), 6.22–6.26 (d, 1H, CH = C*H*COOEt), 6.61–6.65 (t, 1H, benzene proton), 6.71–6.72 (d, 1H, pyrrole H-3 proton), 6.81–6.82 (d, 1H, pyrrole H-4 proton), 7.33–7.36 (d, 1H, PhCOC*H* = CH), 7.58–7.62 (m, 1H, C*H* = CHCOOEt), 7.66–7.78 (m, 3H, PhCOCH = C*H* and benzene protons) ppm; ^{13}C NMR ($CDCl_3$) δ 14.3, 26.8, 28.5, 35.7, 35.9, 37.8, 39.5, 42.7, 53.0, 60.6, 114.4, 115.8, 117.7, 117.8, 117.9 (2C), 123.8, 125.3, 129.5, 129.9, 131.1 (2C), 139.0, 151.4, 167.8, 190.9 ppm; MS (EI): *m*/*z*: 436.22 $(M)^+$.

Procedure for the synthesis of the (E)-3-(5-(E)-(3-(4-(2-norbornylamino)-3-fluorophenyl)-3-oxoprop-1-enyl)-1-methyl-1H-pyrrol-2-yl)-N-hydroxyacrylamide (MC2189) and 3-(5-(3-(3-fluorophenyl)-3-oxoprop-1-enyl)-1-methyl-1H-pyrrol-2-yl)-N-hydroxyacrylamide (MC1568). Example: synthesis of (E)-3-(5-(E)-(3-(4-(2-norbornylamino)-3-fluorophenyl)-3-oxoprop-1-enyl)-1-methyl-1H-pyrrol-2-yl)-N-hydroxyacrylamide (MC2189)

Potassium hydroxide (19.5 mmol, 1.1 g) solution in dry ethanol (5 ml) was added to a hydroxylamine hydro-

chloride (19.5 mmol, 1.35 g) solution in dry ethanol (5 ml) at RT. The mixture was cooled at 0°C, then filtered and to the clear solution 3 (2.1 mmol, 0.9 g) and well-crushed potassium hydroxide (3.65 mmol, 0.2 g) were added. After 1 h, the mixture was diluted with water (50 ml), 2N HCl was slowly added till pH 7 and filtered under vacuum. The solid MC2189 was collected, dried and recrystallized by acetonitrile/methanol; melting point: 219–221°C; yield: 67.3%; ^{1}H NMR (DMSO-d_6) δ1.09 (m, 8H, norbornyl protons), 2.20–2.45 (m, 2H, norbornyl protons), 3.25 (m, 1H, norbornyl proton), 3.70 (s, 3H, NCH_3), 6.10 (bs, 1H, N*H*), 6.25–6.29 (d, 1H, CH = C*H*CONHOH), 6.66–6.68 (m, 2H, pyrrole H-3 proton and benzene proton), 7.11 (pyrrole H-4 proton), 7.45–7.49 (d, 1H, C*H* = CHCONHOH), 7.62–7.85 (m, 4H, PhCOC*H* = CH, PhCOCH = C*H* and benzene protons), 9.00 (bs, 1H, NHO*H*), 10.65 (bs, 1H, N*H*OH) ppm; ^{13}C NMR (DMSO-d_6) δ26.0, 30.8, 34.0, 36.8, 37.4, 41.4, 44.1, 56.4, 104.8, 108.0, 115.6 (2C), 123.2, 124.9, 126.3, 127.4, 127.9, 130.6, 134.8, 136.3, 145.2, 155.4, 161.6, 189.7 ppm; MS (EI): *m*/*z*: 423.20 (M)$^+$.

3-(5-(3-(3-fluorophenyl)-3-oxoprop-1-enyl)-1-methyl-1*H*-pyrrol-2-yl)-*N*-hydroxyacrylamide (MC1568)

Recrystallized by acetonitrile/methanol; melting point: 212–214°C; yield: 68.5%; ^{1}H NMR (DMSO-d_6) δ 3.77 (s, 3H, NCH_3), 6.32–6.36 (d, 1H, CH = C*H*CONHOH), 6.72–6.73 (d, 1H, pyrrole H-3 proton), 7.24–7.25 (pyrrole H-4 proton), 7.42–7.52 (d, 1H, C*H* = CHCONHOH and benzene proton), 7.59–7.69 (m, 2H, PhCOC*H* = CH and benzene proton), 7.77–7.81 (d, 1H, PhCOCH = C*H*), 7.89–7.91 (d, 1H, benzene proton), 7.96–7.98 (d, 1H, benzene proton), 9.00 (bs, 1H, NHO*H*), 10.71 (bs, 1H, N*H*OH) ppm; ^{13}C NMR (DMSO-d_6) δ 37.8, 116.1, 117.7, 117.9 (2C), 119.0, 124.1, 125.3, 125.4, 130.3, 131.1 (2C), 132.7, 137.4, 163.2, 165.9, 190.9 ppm; MS (EI): *m*/*z*: 314.11 (M)$^+$.

Procedure for the synthesis of MS-275 (entinostat)

Triethylamine (1.93 mmol, 0.27 ml) and *O*-(Benzotriazol-1-yl)-*N,N,N′,N′*-tetramethyluronium tetrafluoroborate (0.58 mmol, 0.186 g) were added under nitrogen atmosphere to a solution of4-(((pyridin-3-ylmethoxy)carbonylamino)methyl)benzoic acid **(5)** [24] (0.48 mmol, 0.137 g) in dry *N,N*-dimethylformamide (5 ml), and the resulting mixture was stirred for 15 min. After this time 1,2-phenylendiamine (0.48 mmol, 0.052 g) was added and stirring was continued for a further 30 min. The reaction was quenched by water (20 ml) and the precipitate was filtered, washed with water (3 × 20 ml), and dried. The solid residue was purified by chromatography on silica gel 60 eluting with ethyl acetate to provide MS-275 as a colorless solid, which was recrystallized from acetonitrile; melting point: 159–161°C; yield: 76.6%; ^{1}H NMR (DMSO-d_6) δ 4.24–4.25 (d, 2H, PhCH_2), 4.85 (bs, 2H, NH_2), 5.06 (s, 3-pyridyl-CH_2), 6.54–6.56 (t, 1H, aniline proton), 6.73–6.75 (d, 1H, aniline proton), 6.91–6.95 (t, 1H, aniline proton), 7.12–7.14 (d, 1H, aniline proton), 7.32–7.7.39 (m, 3H, benzene protons and N*H*COO), 7.74–7.76 (d, 1H, pyridine proton), 7.88–7.95 (m, 3H, benzene protons and pyridine proton), 8.50–8.51 (d, 1H, pyridine proton), 8.56 (s, 1H, pyridine proton), 9.58 (bs, 1H, PhCON*H*) ppm; ^{13}C NMR (DMSO-d_6) δ 44.3, 66.3, 118.4, 123.5, 124.1, 124.5, 124.8, 126.6, 127.4 (2C), 127.8 (2C), 133.2, 134.1, 135.6, 142.4, 143.9, 147.5, 148.2, 156.6, 167.0 ppm; MS (EI): *m*/*z*: 376.15 (M)$^+$.

Bioassay

Cell culture & virus

MDCK and NCI-H292 obtained from American Type Culture Collection (ATCC), were grown in Roswell Park Memorial Institute 1640 medium (RPMI 1640) medium supplemented with 10% (v/v) fetal bovine serum (FBS), 0.3 mg/ml glutamine, 100 U/ml penicillin and 100 µg/ml streptomycin. All cells were cultured at 37°C in a 5% CO_2 incubator. Influenza virus A/Puerto Rico/8/34 H1N1 was propagated in the allantoic cavities of 10-day-old embryonated chicken eggs.

Cell infection & viral titration assay

Confluent monolayer of MDCK and NCI-H292 cells were grown in 24-well plates. Cells were infected with PR8 virus at a multiplicity of infection (MOI) of 0.01 for 1 h at 37°C in RPMI without FBS. Cells were treated with different concentration of the inhibitors (0.8 µM [MS-275], 11.7 µM [MC2189] and 15.9 µM [MC1568]), 1 h before, during and after adsorption of PR8 virus to host cells. MC2189, MS-275 and MC1568 compounds were dissolved in dimethyl sulfoxide (DMSO, Sigma Aldrich, MO USA) and diluted to final concentrations in RP medium. The DMSO concentration present in the culture medium was 0.03%. Control cells were treated with DMSO alone at the same concentration present in the test substance being evaluated. Mock infection was performed with the same dilution of allantoic fluid from uninfected eggs. After the viral challenge, mock- and virus-infected cells were washed with phosphate-buffered saline (PBS) and then incubated with medium supplemented with 2% (v/v) FBS for 24, 48 and 72 h at 37°C [40] with or without inhibitors. For infection performed at MOI 1, monolayers of NCI-H292 cells were grown to confluence in 24-well plates and inoculated

with PR8 virus concomitant with different concentration of the inhibitors. The plates were preincubated for 2 h at 4°C to ensure synchronous attachment and entry of the viruses. After the viral challenge, *mock*- and virus-infected cells were washed with PBS and then incubated with medium supplemented with 2% (v/v) FBS for 6 and 8 h at 37°C with or without MC1568, Tubastatin A, as specific HDAC6 inhibitor, and PCI-34051, as specific HDAC8 inhibitor. For each condition, virus production in supernatants of cell cultures was assayed by using hemagglutination assay [41].

HDAC1–6 & HDAC8 isoforms inhibition assay

MC1568 was tested in ten-dose IC_{50} mode with threefold serial dilution starting from 300 µM solution. Individual IC_{50} values for each HDAC isozyme were measured with the homogeneous fluorescence-release HDAC assay. Purified recombinant enzymes were incubated with serial diluted inhibitors at the indicated concentration. The deacetylase activities of HDACs 1–6, and HDAC8 were determined by assaying enzyme activity using AMC-K(Ac)GL (classes I, IIb HDACs) or AMC-K(TFA)GL (class IIa HDACs) substrate as previously described [42,43]. Deacetylated AMC-KGL was sensitive toward lysine peptidase, and free fluorogenic 4-methylcoumarin-7-amide was generated, which can be excited at 355 nm and observed at 460 nm (Reaction Biology Corporation, MD, USA). Data were analyzed on a plate-to-plate basis in relationship to the control and imported into analytical software (GraphPad Prism, CA, USA).

Cell viability assay

The cytotoxicity of MC1568 was evaluated on NCI-H292 and MDCK cells by using a 3-(4,5-dimethylthiazol-2-yl)-2,5-diphenyltetrazolium bromide reduction assay [44]. The cytotoxicity of the compound was calculated as percentage reduction in viable cells with respect to the control culture (cells treated with DMSO alone).

Western blotting analysis

For western blotting analysis, NCI-H292 cells were treated with MC1568 (15.9 µM) 1 h before, during and after adsorption of PR8 virus. Cells were detached, washed with PBS and centrifuged at 700 × *g* for 10 min. The pellet was lysed in cold lysis buffer (10 mM Tris, 150 mM NaCl, 0.25% NP-40, 1 mM phenylmethylsulfonyl fluoride, [pH 7.4]) containing protease and phosphatase inhibitor mixtures (Sigma Aldrich). After 30 min on ice, lysates were centrifuged at 13,000 × *g* for 30 min at 4°C, the supernatants were collected and total protein concentration was determined by Bradford protein assay (Bio-Rad, CA USA).

For the detection of PB1 and PB2 viral polymerases localization, nuclear and cytoplasmic extracts were prepared with NE-PER Nuclear and Cytoplasmic extraction kit (Pierce, Thermo Fisher Italy), and protein concentrations were determined using BCA Protein Assay Kit (Pierce, Thermo Fisher, MA USA). Same amount of protein of nuclear and cytoplasmic extracts were resuspended in Laemmli loading buffer, separated with SDS-PAGE (the percentage of acrylamide used ranging from 7.6 to 12%, according to the molecular weight of protein of interest). The membranes were blocked with 10% nonfat dry milk in Tris-buffered saline containing 0.1% Tween-100 for 1 h at RT. Primary antibodies, used at final concentration of 1 µg/ml, overnight at 4°C, included goat polyclonal anti-influenza A virus IgG (Chemicon), goat polyclonal anti-PB1 and goat polyclonal anti-PB2 (Santa Cruz, sc-17601 and sc-17603), mouse monoclonal antiactin (Sigma Aldrich) and mouse monoclonal anti-lamin A/C (BD Biosciences, NJ USA). Then the membranes were incubated with secondary antibodies (horseradish-peroxidase conjugated, Jackson ImmunoResearch Europe, UK) for 1 h at RT and developed with the Pierce ECL Plus Western Blotting Substrate (Thermo Scientific). Densitometry was done using Quantity One 1-D Analysis software (Bio-Rad); β-actin and lamin were used as loading control.

Immunoprecipitation assay

For acetylated-lysine Hsp90 immunoprecipitation, NCI-H292 cells were plated for 24 h at a density of 4 × 10^6 cells/well and treated with MC1568 (15.9 µM) 1 h before, during and after adsorption of PR8 virus (MOI 1). One hour and 3 h after infection, cells were harvested and lysed in acetylated-lysine buffer (20 mM Tris, pH 7.5, 150 nM NaCl, 1 mM EDTA, 1 mM EGTA, 1% Triton X-100, 2.5 mM sodium pyrophosphate, 1 mM β-glycerophosphate, 1 mM sodium orthovanadate, 5 mM sodium butyrate, 1 mM phenylmethylsulfonyl fluoride and protease inhibitor cocktail; all reagents were purchased from Sigma). A total of 500 µg of protein from each sample was precleared with 15 µl of protein A/G Plus-Agarose (Santa Cruz Biotechnology) for 60 min at 4°C. Antiacetyl-lysine antibody (1 mg/ml; Cell Signaling Technology) was then added to the samples and incubated at 4°C overnight. Protein A/G Plus-Agarose (30 µl/sample) was added to the lysates and incubated for 3 h at 4°C. After several washes, immunocomplexes were resuspended in Laemmli loading buffer and heated at 100°C for 10 min before immunoblot analysis with anti-Hsp90 antibody (Abcam). Then, membranes were stripped and reprobed with antiacetylated-lysine antibody as control. Parallely, total cell lysates were analyzed by western blot with Hsp90, acetyltubulin (Sigma) and β-actin (Sigma) antibodies.

The relative levels of acetylated Hsp90 were calculated as ratio between densitometric values of Hsp90 from acetylated-lysine IP and Hsp90 from the total lysate for each sample.

Immunofluorescence assay

Immunofluorescence assay was performed as previously described [45]. NCI-H292 cells were plated for 24 h at density of 1 × 10^4 cells/well. Cells were treated with MC1568 (15.9 μM) 1 h before, during and after adsorption of PR8 virus (MOI 1). One and 3 h after viral challenge, cells were fixed with 4% paraformaldehyde in PBS for 15 min at RT. After being permeabilized (10-min incubation with 0.3% Triton X-100 [Sigma, MO USA] in PBS), the cells were incubated for 20 min with 0.3% bovine serum albumin (Sigma) in PBS to block nonspecific binding sites and then overnight at 4°C with rabbit anti-Hsp90 (Abcam, 1:100) and mouse anti-Hsp90 acetyl K294 (Rockland, 1:500) antibodies. The next day, cells were incubated for 90 min at RT with Alexa Fluor 633 goat anti-rabbit (1:1000; Invitrogen); Alexa Fluor 488 goat antimouse (1:1000; Invitrogen). Finally, nuclei were counterstained with propidium Iodide/RNase for 30 min at RT and the cells were coverslipped with ProLong Gold antifade reagent (Invitrogen, Thermo Fisher Scentific, MA USA).

Images (512 × 512 pixels) were acquired at 63× magnification with a confocal laser scanning system (TCS-SP2, Leica Microsystem, Wetzlar, Germany) and an oil-immersion objective (N.A. 1.4; physical pixel size: 233 nm), additional 3× magnification was applied. Fluorescent dyes were excited with Ar/ArKr laser (for 488 nm) or HeNe lasers (for 543 and 633 nm). All experiments were repeated at least three-times, and at least ten randomly chosen microscopic fields were analyzed for each condition.

Variations in Hsp90 acetylation were quantified as the ratio between the sums of fluorescence intensities in every pixel of recorded field for Hsp90 acetyl K294 and Hsp90. Values were then normalized to controls (that was set equal to 1). In every studied condition negative controls were obtained by omitting the primary antibody. The operator was blinded to the study conditions.

RNA extraction & real-time PCR

Total RNA was isolated using the RNeasy Mini kit (Qiagen) following the manufacturer's protocol. An equal amount of the total RNA was used as template to generate cDNA using iScriptcDNA Synthesis Kit (Bio-Rad). An aliquot of the cDNA was then subjected to 40 cycles of Real-time PCR amplification (95°C, 10 s; 60°C, 30 s) using the iQ SYBR Green Supermix and LightCycleriQ 5 (Bio-Rad). qPCR was performed in duplicate by using the following primers set: HA forward (5′-TGTATAGGCTACCATGCGAAC-3′) and reverse (5′-TTCCGTTGTGGCTGTCTTC-3′); NP forward (5′CGTCCCAAGGCACCAAAC-3′) and reverse (5′-AATCGTCCAATTCCAC-CAATC-3′); M1 forward (5′-GCAAGCGATGAGA-ACCATTGG-3′) and reverse (5′GCGGCAATAGC-GAGAGGATC-3′); and housekeeping 18|S forward (5′-TCACCAGGTCCAGACACAATA-3′) and reverse (5′AAGCAGACAAATCACTCCACC-3′), β-actin forward (5′ACCAACTGGGACGACATGGAGAAA-3′) and reverse (5′TAGCACAGCCTGGATAGCAAC-GTA-3′); GAPDH forward (5′GTCGGAGTCAACG-GATTT-3′) and reverse (5′CAACAATATCCACTT-TACCAGAG-3′) genes. The results are presented as fold difference relative to control.

Statistical analysis

All tests were carried out in triplicate and the results were averaged. Data were expressed as the mean ± SD. The statistical significance between different experimental conditions was determined by the paired Student's t-test. One-way analysis of variance test followed by Bonferroni's *post-hoc* test was used for multiple comparisons (p-values of <0.05 were considered significant).

Results & discussion

Chemistry

4-(2-norbornylamino)-3-fluoroacetophenone **1** [46] was synthesized by treating 3,4-difluoroacetophenone with 2-norbornylamine and potassium carbonate at 90°C overnight. Aldehyde **2**, prepared through a Vilsmeyer-Haack reaction performed on (*E*)-ethyl 3-(1-methyl-1*H*-pyrrol-2-yl)acrylate [47] by using oxalyl chloride and *N,N*-dimethylformamide at 0°C in dichloromethane, was treated with **1** or with 3-fluoroacetophenone using sodium ethoxide in ethanol to afford corresponding esters **3** and **4**. Such esters were directly converted into the hydroxamates MC2189 and MC1568 by reaction with hydroxylamine and potassium hydroxide in ethanol (Figure 1). MS-275 was prepared by treating acid **5** [48] with *O*-(Benzotriazol-1-yl)-*N,N,N′,N′*-tetramethyluronium tetrafluoroborate, triethylamine and 1,2-phenylendiamine in *N,N*-dimethylformamide and under nitrogen atmosphere (Supplementary Figure 1). Tubastatin A and PCI-34051 were prepared according to the procedures previously described [49,50].

Evaluation of HDACis effects on PR8 virus replication in MDCK & NCI-H292 cells

To investigate the potential anti-influenza activity of HDACis, with different selectivity for the various deacetylase isoform, we tested the following compounds: MC2189, able to inhibit HDAC1, 4 and 6 (representative

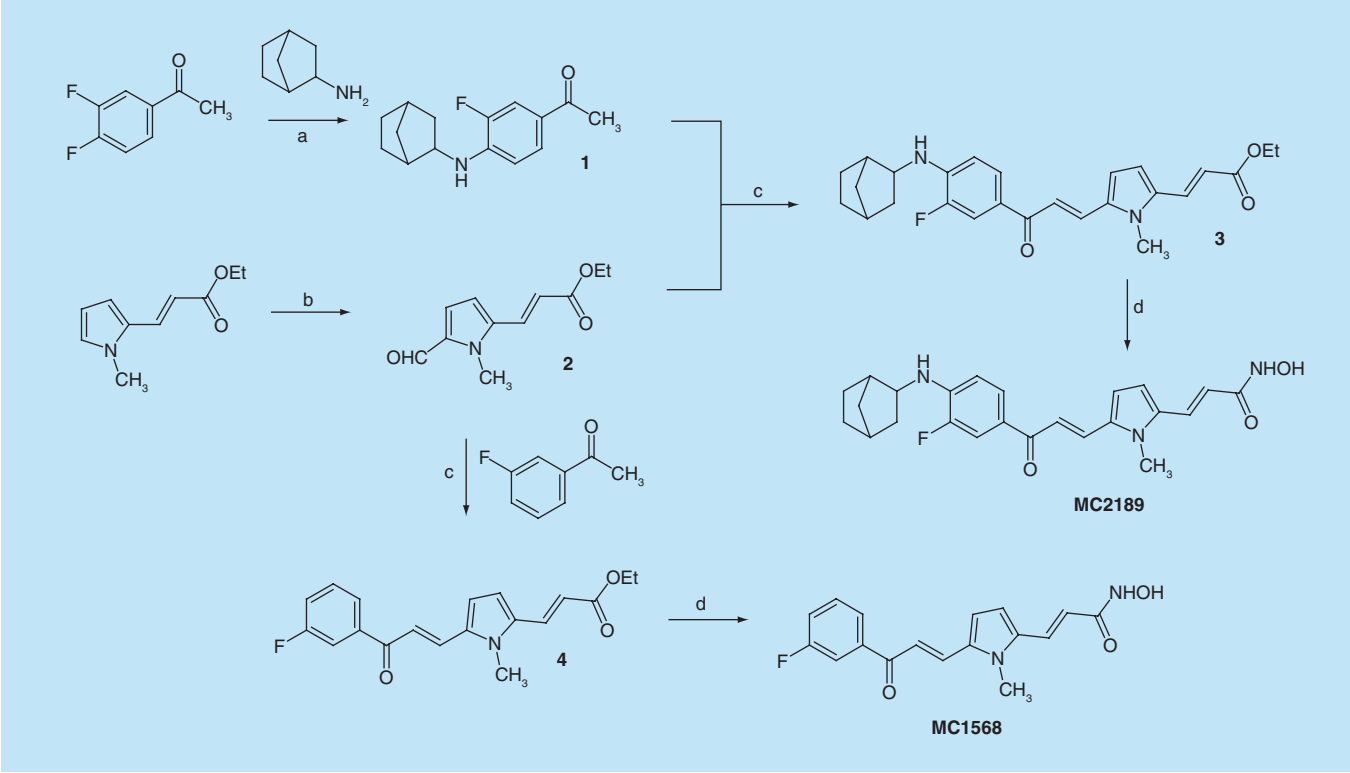

Figure 1. Synthesis of MC2189, MC1568. Reagents and conditions: a: K2CO3, dry DMF, 90°C, overnight; b: **(1)** (COCl)2, dry DMF, CH2Cl2, 0°C, 1 hour, **(2)** 2N NaOH, 10 min; c: Na (metal), dry EtOH, 5 hours; d: NH2OH, KOH, ethanol, 1 hour.

of class I, class IIa and class IIb HDACs, respectively) [49] (3f in the reference paper); MS-275, able to inhibit only HDAC1–3 and not HDAC8 [51], and MC1568, a class II-selective HDAC inhibitor, studied in a number of different cellular contexts [24–37,52]. As a pan-HDACi, we decided to use MC2189 that is a quite weak inhibitor [46] with respect to the more potent Tricostatin A (TSA) and SuberoylAnilide Hydroxamic Acid (SAHA) because these latter caused a significant cytoxicity in our models (data not shown). Highly permissive MDCK cells were infected with PR8 virus at low MOI to allow multiple cycles of viral replication and viral titer was evaluated 24, 48 and 72 h postinfection (p.i.).

As shown in Figure 2A (left and right panels) MS-275 did not significantly affect PR8 virus replication, or slightly increased it, as expected by an efficient HDAC1 inhibitor [17]. MC2189 caused a reduction ranging between 50 and 33.3% after 72 h p.i. (Figure 2A & Figure 2B). Interestingly, the treatment with MC1568 strongly reduced viral titer 24 h p.i (95.25% decrease $p < 0.0001$), with respect to infected controls. The antiviral effect was partly lost 48 and 72 h p.i., when the viral yield was inhibited by 38 ($p < 0.05$) and 33.3%, respectively (Figure 2A & B). The dose-response curve, performed 24 h p.i., showed a significant inhibition of viral replication at concentration ≥6.4 μM ($p < 0.0001$) (Figure 2C). To exclude the possibility that the observed antiviral activity of MC1568 was due to its toxic effect on host cells, the 3-(4,5-dimethylthiazol-2-yl)-2,5-diphenyltetrazolium bromide assay in MDCK cells was performed. As shown in Figure 2D, no significant toxic effect was detectable at the concentration able to inhibit viral replication, according with previous studies performed in other contexts [31,36].

Since HDAC activity is species-specific, we decided to continue our experiments on a human cell line: pulmonary epithelial cells (NCI-H292). Also in this model, MC1568-treatment, at the concentration of 15.9 μM induced a significant reduction (75.2%; $p < 0.0001$) of viral replication, 24 h p.i. (Figure 3A & B). The inhibition of viral replication was less evident, 48 and 72 h p.i., when we found 33.3 and 37.5% reduction, respectively. No inhibition of viral replication was observed at concentration less to 3.2 μM (Figure 3C). No significant cytotoxic effect was detectable at concentration of 15.9 μM (Figure 3D).

We then investigated, the effect of MC1568 on viral protein expression. The results showed that, MC1568 treatment reduced the expression of viral protein compared with that of untreated controls (Figure 3E), 24 h p.i. In particular, densitometric analysis revealed a significant reduction ($p < 0.05$) in the expression of hemagglutinin (HA), NP and matrix protein M1 (Figure 4E, right panel). Overall these results showed

that MC1568 was able to inhibit PR8 virus replication 24 h p.i., while such an effect decreased later in infection. The addition of fresh compound after the first 24 h, did not increase the antiviral effect measured 48 and 72 h p.i. (data not shown). These data let us to speculate that the increased viral production, observed 48 and 72 h p.i., might be also related to a 'secondary' effect of MC1568 in inducing microtubules hyperacetylation that, after the first block, increases the trafficking of the produced viral components to plasma membrane, and the consequent viral release [20,21].

Determination of human HDAC isoform selectivity of MC1568

On the basis of these results, to investigate the mechanisms underlying the MC1568 antiviral effect, we tested MC1568 in ten-dose IC_{50} mode with threefold serial dilution starting from 300 µM solution against the most biologically relevant HDAC isoenzymes (HDAC1–6 and HDAC8). MC1568 has been typically used in many different cellular contexts as a class II-selective HDACi [24–37,52].

It has been previously reported that MC1568 produced a modest hyperacetylation of histone 4 and was ineffective on the other histones in HT29 cells [30]. Although these data have been obtained in a different cell line and considering a cellular selectivity for histone acetylation, they might be extended to NCI-H292 and MDCK cells, used in our experimental models. In Table 1, we reported data on enzymatic inhibition of MC1568, MC2189, Tubastatin A, PCI-34051, MS275, Tricostatin and SAHA, against different HDAC isoforms. The results showed that IC_{50} values fully confirmed the behavior of MC1568 as class II-selective HDACi, but in addition clearly revealed that MC1568 was also able to inhibit HDAC8 at single-digit micromolar level. This is not surprising, because its 3-chloro analogue, MC1575, was previously found active against HDAC8 and FB188 HDAH, a bacterial HDAC-like amidohydrolase with 35% similarity to human HDAC6, at low µM levels [53]. Therefore, antiviral activity could be explained, at least in part, by efficient dual HDAC6/HDAC8 inhibition by MC1568. The same treatment made with MC2189, a

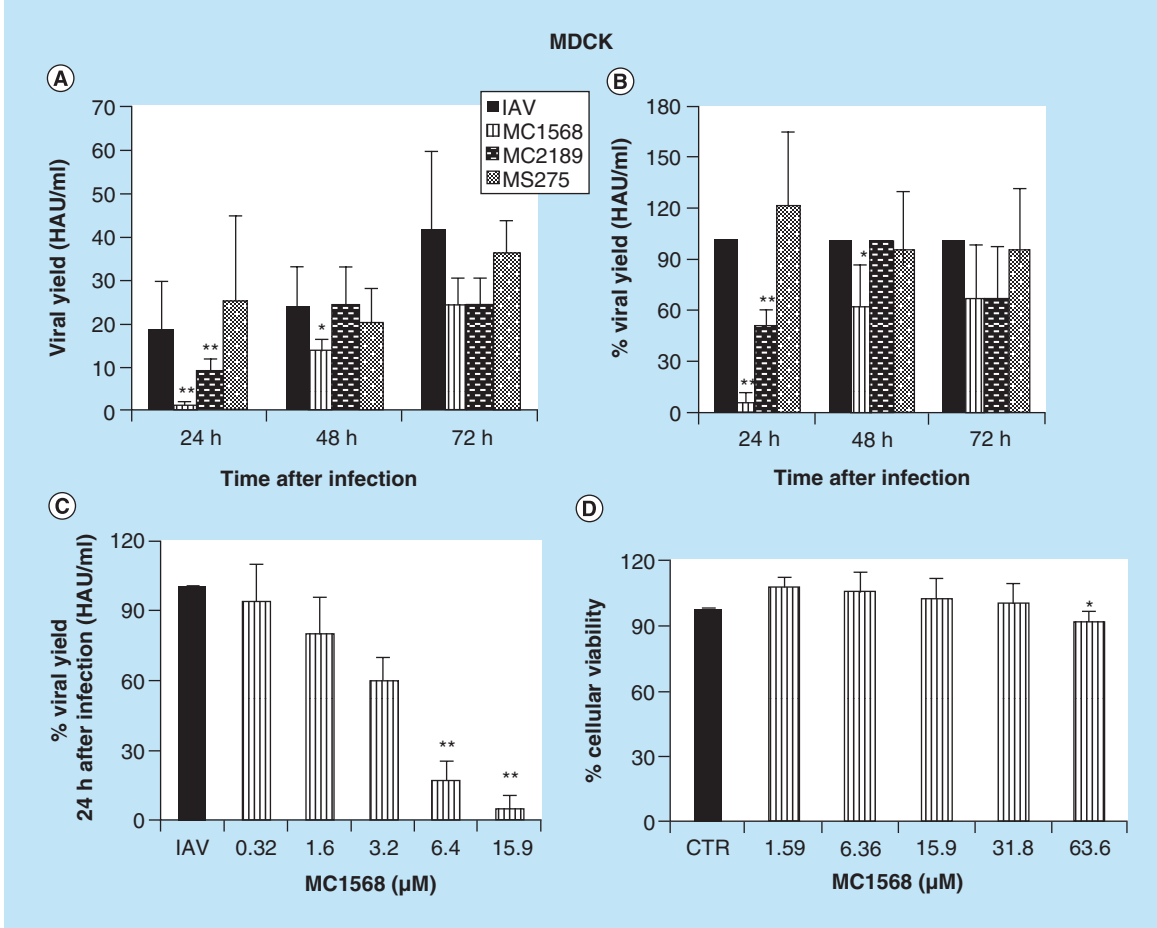

Figure 2. Effects of different HDACi (MS-275, MC2189, MC1568) on PR8 virus replication in MDCK cells.
IAV: Influenza A virus.

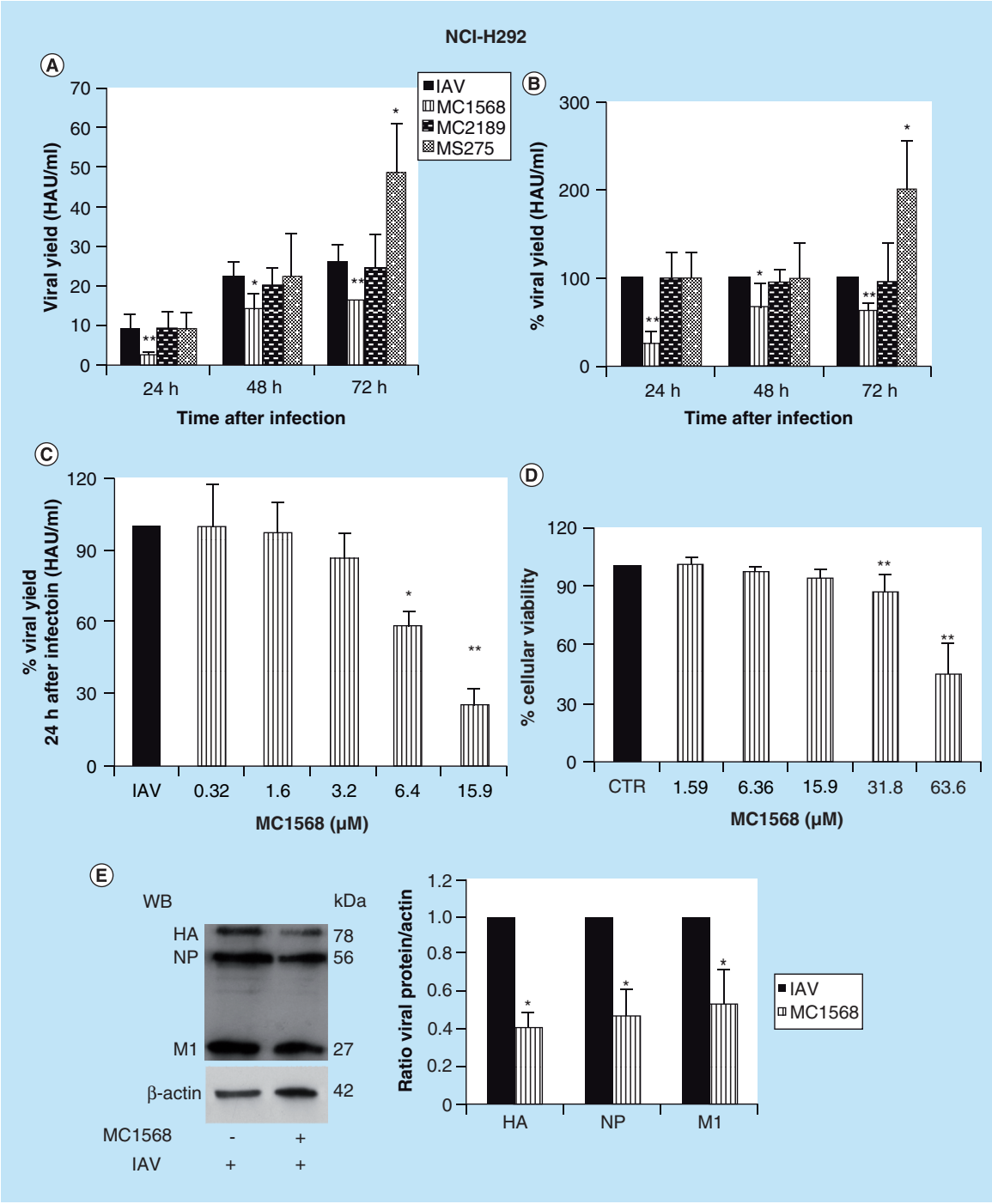

Figure 3. Effects of different HDACi (MS-275, MC2189, MC1568) on PR8 virus replication in NCI-H292 cells.
HA: Hemagglutinin; IAV: Influenza A virus; NP: Nucleoprotein.

pan-HDAC inhibitor, displayed reduction of virus titer only in MDCK cells, and the use of MS-275, a class I-selective HDACi able to inhibit HDAC1–3 and not HDAC8, showed no effect on MDCK and NCI-H292 cells or significantly increased PR8 virus replication ($p < 0.05$; Figures 2A & B and Figure 3A & B) in agreement with the opposite roles exerted by HDAC1 and HDAC8 in IAV infection [17].

Characterization of MC1568 antiviral effect in a single replication cycle in NCI-H292 cells

To clarify the mechanism/s potentially involved in MC1568 antiviral effect, NCI-H292 cells were infected with PR8 virus at MOI 1, to allow a single virus replication cycle, and treated with MC1568. In order to synchronize the entry of viral particles, the attachment to the cells was carried out at 4°C to allow

virus binding and prevent viral entry, that was induced by shift at 37°C. According with previously standardized methods [7], the viral release was measured in supernatant 6 and 8 h after infection. The addition of MC1568 caused a 75 and 77.1% reduction of viral titer 6 h p.i. ($p < 0.005$) and 8 h p.i. ($p < 0.005$), respectively

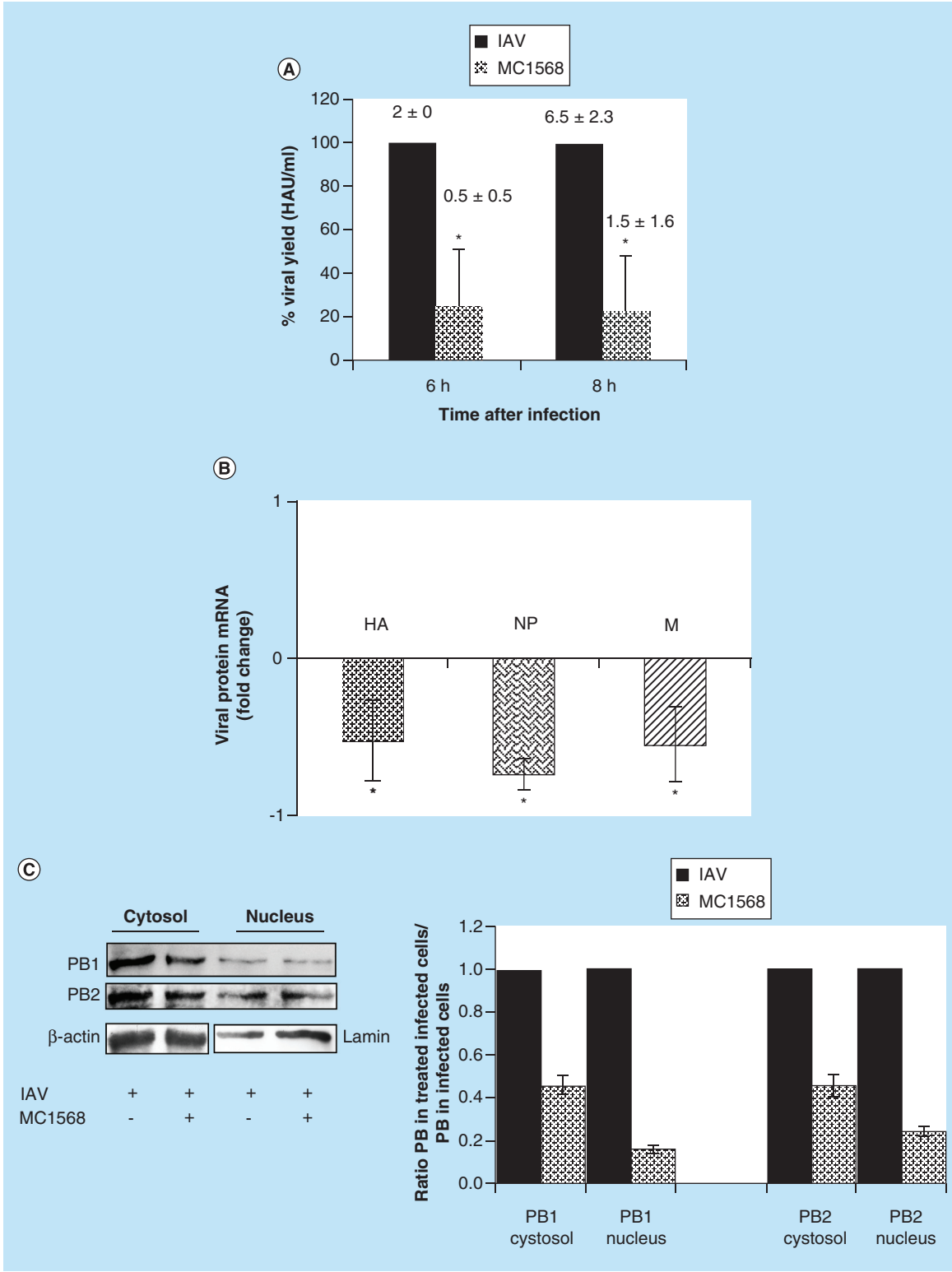

Figure 4. Effect of MC1568 treatment on viral polymerase expression and viral mRNA levels.
HA: Hemagglutinin; IAV: Influenza A virus; NP: Nucleoprotein.

Table 1. IC_{50} values of MC1568, MC2189 and the known TSA and SAHA (pan-HDAC inhibitors), MS275 (Class I HDAC inhibitor), Tubastatin A (HDAC6 inhibitor) and PCI-34051 (HDAC8 inhibitor) against human HDAC1, HDAC2, HDAC3, HDAC4, HDAC5, HDAC6 and HDAC8.

Compound	IC_{50}, μM						
	Class I			Class IIa		Class IIb	Class I
	HDAC1	HDAC2	HDAC3	HDAC4	HDAC5	HDAC6	HDAC8
MC1568	>300	>300	>300	48.2	25.3	5.94	1.81
MC2189	8.2	12.5	13.9	17.3	22.9	8.3	9.2
Tubastatin A†	16.4	>30	>30	>30	>30	0.015	0.85
PCI-34051‡	4	>50	>50	ND	ND	2.9	0.01
MS275§	0.181	1.155	2.311	>10	ND	>10	>10
TSA	0.007	0.010	0.011	7.3	2.8	0.001	0.11
SAHA	0.31	0.24	0.13	76	27.2	0.02	0.31

†Data taken with permission from [49].
‡Data taken with permission from [54].
§Data taken with permission from [51].

(Figure 4A). To investigate the mechanisms underlying such an effect, we then analyzed, 6 h after infection, the mRNA levels for, HA, NP and M proteins. This time has been chosen to obtain high levels of mRNAs before the peak of viral replication. In this condition, the rate of all mRNAs was significantly ($p < 0.05$) diminished in cells treated with MC1568 (Figure 4B).

Nuclear localization of PB1 and PB2 polymerase subunits represents an essential condition for the transcription of viral RNAs, including mRNAs [2]. It is known that assembly and nuclear import of IAV polymerase subunits is regulated by Hsp90 [39], which, together with tubulin, are the main targets of HDAC6 [55,56], an HDAC isoform inhibited by MC1568. We then decided to analyze the cytosolic and nuclear content of PB1 and PB2 following MC1568 treatment. As shown in Figure 4C, the expression of PB1 and PB2, at both cytosolic and nuclear level, are substantially reduced after treatment. In addition, the densitometric analysis indicate that the nuclear content of proteins was decreased by 84.2 and 75.9% for PB1 and PB2, respectively, when compared with untreated cells. These data suggest that the reduced expression of viral proteins and their mRNA, observed following MC1568 treatment may be, at least in part, related to the low nuclear content of PB1 and PB2. Since we showed that MC1568 was able to inhibit HDAC8, other than HDAC6 activity, we cannot exclude the possibility that the low nuclear polymerase levels that we found, could be related to an inhibition of HDAC8 related effects, such as endosome acidification and/or vRNP nuclear import, as previously reported by Yamauchi *et al.* [17]. To test the potential antiviral activity of compounds with a similar enzyme inhibition profile, we checked, in the same experimental model (NCI infected cells), the effect of HDAC6 inhibitor Tubastatin A and HDAC8 inhibitor PCI-34051. On the basis of data on their enzymatic inhibition on HDAC6 and 8 (Table 1), we decided to assess the antiviral activity of three concentrations: 0.01, 0.1 and 1 μM. We found that both compounds were able to partially inhibit influenza virus replication, only at the concentration of 1 μM. The analysis of viral titer in the supernatant of infected cells, performed 6 h p.i., showed a slight reduction of viral replication (27.67 and 33.92% in Tubastatin A and PCI-34051 treated cells, respectively) (Supplementary Figure 2), suggesting that the higher MC1568's effects might be related to a dual HDAC6/8 inhibitory effect. In addition, it is possible to hypothesize that the inhibition of HDAC6 activity may be responsible for Hsp90 hyperacetylation, decreasing its chaperone activity for nuclear entry of viral polymerases. For this reason, in the next set of experiments, we analyzed the acetylation status of Hsp90 after MC1568 treatment.

Evaluation of Hsp90 acetylation state in NCI-H292 cells during PR8 virus infection and MC1568 treatment

In order to analyze the effect of MC1568 on Hsp90 acetylation we performed immunoprecipitation assay from NCI-H292 cells. As a control, we checked the acetylation of tubulin, a known target of HDAC6 activity. The results shown in Figure 5A revealed that the treatment with MC1568 caused an increase in Hsp90 acetylation, 1 and 3 h p.i. Interestingly, we noted that PR8 virus itself was able to induce Hsp90 hyperacetylation 3 h after viral infection (Figure 5A).

Hsp90 can be acetylated at different sites [57]. One of these was mapped to Lys 294 [55,56], and it was deacetylated by HDAC6 [57]. Acetylation of K294 plays an

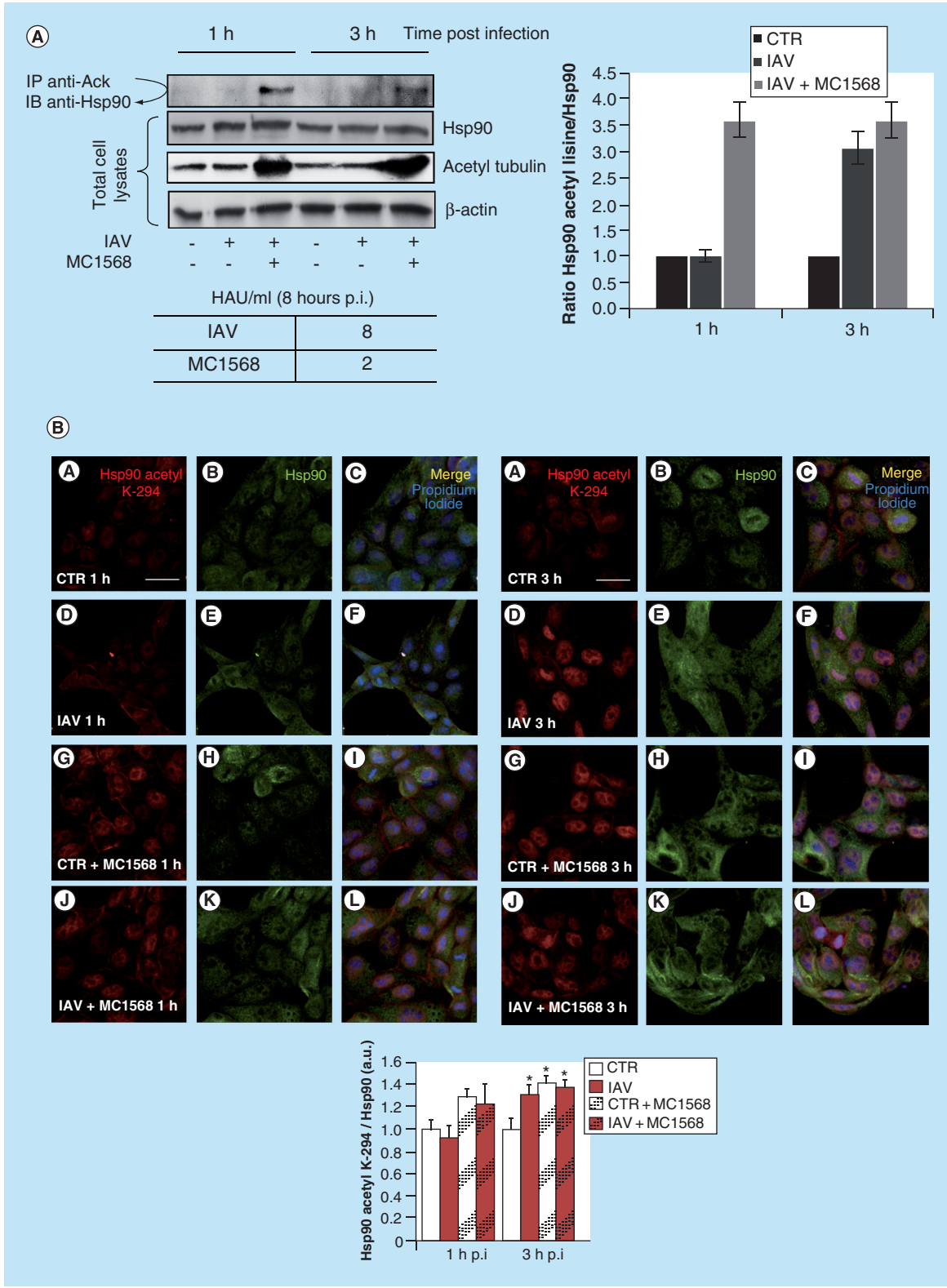

Figure 5. Analysis of Hsp90 acetylation state in PR8 virus infected and MC1568 treated NCI-H292 cells.
IAV: Influenza A virus.

important role in regulating the Hsp90 functions [55]. In order to clarify the effect of MC1568 and PR8 virus on K294 acetylation, we performed an immunofluorescence analysis with a specific antibody against Hsp90 α acetyl-K294. As shown in Figure 5B, MC1568 treatment induced an increase in Hsp90 acetylation which starts from 1 h p.i. As already shown by immunoprecipitation, the virus itself, induced Hsp90 K294-hyperacetylation which was evident only 3 h p.i. These data were confirmed by quantification of fluorescence intensity (Figure 5B, bottom). Acetylated Hsp90 was detected in infected cells also later (6 h p.i., data not shown), suggesting that virus-induced Hsp90 acetylation it is not just a transient event. Further studies are needed to better define the extent, the functional role and the mechanisms involved in this phenomenon. Nevertheless, overall data let us to speculate that the early hyperacetylating effect, observed after MC1568 treatment, might play a pivotal role in determining the decrease of Hsp90 chaperone activity, necessary for nuclear entry of viral polymerases. The consequent decrease of PB1 and PB2 intranuclear levels might be responsible for the decrease in mRNA transcription and viral protein expression and might explain, at least in part, its anti-influenza activity.

Conclusion

In summary, we show that HDAC6/8 inhibitor MC1568 exerts a significant anti-influenza effect. These findings provide further insights on the role of the acetylation in modifying function of host-cell proteins that are involved in regulating influenza virus life-cycle.

Future perspective

Currently used anti-influenza drugs have limited effectiveness due to their toxicity and the almost inevitable selection of drug-resistant viral mutants [3]. For this reason, many efforts have been recently devoted to the search of new targets for novel effective compounds. The life-cycle of viruses strictly depends on structures and signaling pathways of the host cells in which they are replicating. In this context, post-translational modifications of proteins, such as acetylation, may play a pivotal role in regulating viral replication and the outcome of infection [16,17,21]. A better understanding of the mechanisms underlying the anti-influenza effects of MC1568 could lead to the discovery of novel targets for anti-influenza drugs.

Supplementary data

To view the supplementary data that accompany this paper, please visit the journal website at: www.future-science.com/doi/full/10.4155/fmc-2016-0073

Acknowledgements

The authors thank M Aleandri and R Piacentini for their technical support during microscopy and image analysis.

Financial & competing interests disclosure

This research was financially supported by the Italian Ministry of Instruction Research PON 0101802 grant (AT Palamara), PRIN 2010PHT9NF005 grant (L Nencioni), FIRB RBFR10ZJQT grant (A Mai), RF-2010–2318330 (A Mai) grant, IIT-Sapienza Project (A Mai), and FP7 Projects BLUEPRINT/282510 and A-PARADDISE/602080 (A Mai). The authors have no other relevant affiliations or financial involvement with any organization or entity with a financial interest in or financial conflict with the subject matter or materials discussed in the manuscript apart from those disclosed.

No writing assistance was utilized in the production of this manuscript.

Executive summary

HDACis effects on PR8 virus replication in epithelial cells

- Treatment with MC1568 (HDAC inhibitor) induces a significant reduction of H1N1 influenza A virus replication.

Determination of human HDAC isoform selectivity of MC1568

- MC1568 is able to inhibit HDAC8 at single-digit micromolar level in addition to class II HDACs.

Characterization of MC1568 activity in NCI-H292 infected cells

- MC1568 treatment reduces intranuclear content of viral polymerases PB1 and PB2, a limiting condition for viral RNA transcription.
- At concentration able to inhibit HDAC6 and HDAC8 activity, MC1568 treatment induces Heat shock protein 90 (Hsp90) lysine acetylation.

References

Papers of special note have been highlighted as:
• of interest; •• of considerable interest

1 Vasin AV, Temkina OA, Egorov VV, Klotchenko SA, Plotnikova MA, Kiselev OI. Molecular mechanism enhancing the proteome of influenza A viruses: an overwiew of recently discovered proteins. *Virus Res.* 185, 53–63 (2014).

2 Palese P, Shaw ML. Orthomyxoviridae: the viruses and their replication. In: *Fields Virology* (Volume 2). Knipe DM, Howley P (Eds). Lippincott Williams & Wilkins, PA, USA, 1691–1740 (2013).

3 Lee SM, Yen HL. Targeting the host or the virus: current and novel concepts for antiviral approaches against influenza virus infection. *Antiviral Res.* 96(3), 391–404 (2012).

4 Saladino R, Barontini M, Crucianelli M, Nencioni L, Sgarbanti R, Palamara AT. Current advances in anti-influenza therapy. *Curr. Med. Chem.* 17(20), 2101–2140 (2010).

5 Sgarbanti R, Nencioni L, Amatore D *et al.* Redox regulation of the influenza hemagglutinin maturation process: a new cell-mediated strategy for anti-influenza therapy. *Antioxid. Redox Signal.* 15(3), 593–606 (2011).

6 Nencioni L, De Chiara G, Sgarbanti R *et al.* Bcl-2 expression and p38MAPK activity in cells infected with influenza A virus: impact on virally induced apoptosis and viral replication. *J. Biol. Chem.* 284(23), 16004–16015 (2009).

7 Palamara AT, Nencioni L, Aquilano K *et al.* Inhibition of influenza A virus replication by resveratrol. *J. Infect. Dis.* 191(10), 1719–1729 (2005).

8 Yang XJ, Seto E. Lysine acetylation: codified crosstalk with other posttraslational modifications. *Mol. Cell* 31(4), 449–461 (2008).

9 Falkenberg KJ, Johnstone RW. Histone deacetylases and their inhibitors in cancer, neurological diseases and immune disorders. *Nat. Rev. Drug Discov.* 13(9), 673–691 (2014).

10 Clocchiatti A, Florean C, Brancolini C. Class IIa HDACs: from important roles in differentiation to possible implications in tumorigenesis. *J. Cell. Mol. Med.* 15(9), 1833–1846 (2011).

11 Yang PH, Zhang L, Zhang YJ, Zhang J, Xu WF. HDAC6: physiological function and its selective inhibitors for cancer treatment. *Drug Discov. Ther.* 7(6), 233–242 (2013).

12 Yan J. Interplay between HDAC6 and its interacting partners: essential roles in the aggresome-autophagy pathway and neurodegenerative diseases. *DNA Cell Biol.* 33(9), 567–580 (2014).

13 Rotili D, Simonetti G, Savarino A, Palamara AT, Migliaccio AR, Mai A. Non-cancer uses of histone deacetylase inhibitors: effects on infectious diseases and beta-hemoglobinopathies. *Curr. Top. Med. Chem.* 9(3), 272–291(2009).

14 Das Gupa K, Shakespear MR, Iyer A, Fairlie DP, Sweet MJ. Histone deacetylases in monocyte/macrophage development, activation and metabolism: refining HDAC targets for infiammatory and infectious diseases. *Clin. Transl. Immunol.* 5(1), e62 (2016).

15 Savarino A, Mai A, Norelli S *et al.* 'Shock and kill' effects of class I-selective histone deacetylase inhibitors in combination with the glutathione synthesis inhibitor buthionine sulfoximine in cell line models for HIV-1 quiescence. *Retrovirology* 6, 52 (2009).

16 Guise AJ, Budayeva HG, Diner BA, Cristea IM. Histone deacetylases in herpesvirus replication and virus-stimulated host defense. *J. Viruses* 5(7), 1607–1632 (2013).

17 Yamauchi Y, Boukari H, Banerjee I, Sbalzarini IF, Horvath P, Helenius A. Histone deacetylase 8 is required for centrosome cohesion and influenza A virus entry. *PLoS Pathog.* 7(10), e1002316 (2011).

•• **Very interesting research article regarding the role of HDAC8 in influenza A virus (IAV) entry into host cell.**

18 Banerjee I, Miyake Y, Nobs SP *et al.* Influenza A virus uses the aggresome processing machinery for host cell entry. *Science* 346(6208), 473–477 (2014).

•• **Very interesting research article about the involvement of HDAC6 in IAV entry into host cell.**

19 Husain M, Harrod KS. Influenza A virus-induced caspase-3 cleaves the histone deacetylase 6 in infected epithelial cells. *FEBS Lett.* 583(15), 2517–2520 (2009).

•• **Very interesting research article regarding the deacetylase activity of HDAC6 during IAV replication.**

20 Husain M, Harrod KS. Enhanced acetylation of alpha-tubulin in influenza A virus infected epithelial cells. *FEBS Lett.* 585(1), 128–132 (2011).

21 Husain M, Cheung CY. Histone deacetylase 6 inhibits influenza A virus release by downregulating the trafficking of viral components to the plasma membrane via its substrate, acetylated microtubules. *J. Virol.* 88(19), 11229–11239 (2014).

22 Mai A, Rotili D, Massa S *et al.* Discovery of uracil-based histone deacetylase inhibitors able to reduce acquired antifungal resistance and trailing growth in *Candida albicans*. *Bioorg. Med. Chem. Lett.* 17(5), 1221–1225 (2007).

23 Simonetti G, Passariello C, Rotili D, Mai A, Garaci E, Palamara AT. Histone deacetylase inhibitors may reduce pathogenicity and virulence in *Candida albicans*. *FEMS Yeast Res.* 7(8), 1371–1380 (2007).

24 Mai A, Massa S, Pezzi R *et al.* Class II (IIa)-selective histone deacetylase inhibitors. 1. Synthesis and biological evaluation of novel (aryloxopropenyl)pyrrolyl hydroxyamides. *J. Med. Chem.* 48(9), 3344–3353 (2005).

25 Inoue S, Mai A, Dyer MJS, Cohen GM. Inhibition of histone deacetylase Class I but not Class II Is critical for the sensitization of leukemic cells to tumor necrosis factor-related apoptosis-induced apoptosis. *Cancer Res.* 66(13), 6785–6792 (2006).

26 Duong V, Bret C, Altucci L *et al.* Specific activity of class II histone deacetylases in human breast cancer cells. *Mol. Cancer Res.* 6(12), 1908–1119 (2008).

27 Scognamiglio A, Nebbioso A, Manzo F, Valente S, Mai A, Altucci L. HDAC-class II specific inhibition involves HDAC proteasome-dependent degradation mediated by RANBP2. *Biochim. Biophys. Acta* 1783(10), 2030–2038 (2008).

28 Ragno R, Simeoni S, Rotili D *et al.* Class II-selective histone deacetylase inhibitors. Part 2: alignment-independent GRIND 3-D QSAR, homology and docking studies. *Eur. J. Med. Chem.* 43(3), 621–632 (2008).

29 Illi B, Dello Russo C, Colussi C *et al.* Nitric oxide modulates chromatin folding in human endothelial cells via protein phosphatase 2A activation and class II histone deacetylases nuclear shuttling. *Circ. Res.* 102(1), 51–58 (2008).

30 Naldi M, Calonghi N, Masotti L *et al.* Histone post-translational modifications by HPLC-ESI-MS after HT29 cell treatment with histone deacetylase inhibitors. *Proteomics* 9(24), 5437–5445 (2009).

31 Nebbioso A, Manzo F, Miceli M *et al.* Selective class II HDAC inhibitors impair myogenesis by modulating the stability and activity of HDAC-MEF2 complexes. *EMBO Rep.* 10(7), 776–782 (2009).

32 Nebbioso A, Dell'Aversana C, Bugge AK *et al.* HDACs class II selective inhibition alters nuclear receptor dependent differentiation. *J. Mol. Endocrinol.* 45(4), 219–228 (2010).

33 Colussi C, Rosati J, Straino S *et al.* N^{ε}-lysine acetylation determines dissociation from GAP junctions and lateralization of connexin 43 in normal and dystrophic heart. *Proc. Natl Acad. Sci. USA* 108(7), 2795–2800 (2011).

34 Lenoir O, Flosseau K, Ma FX *et al.* Specific control of pancreatic endocrine beta- and delta-cell mass by class IIa histone deacetylases HDAC4, HDAC5, and HDAC9. *Diabetes* 60(11), 2861–2871 (2011).

35 Palmisano I, Della Chiara G, D'Ambrosio RL *et al.* Amino acid starvation induces reactivation of silenced transgenes and latent HIV-1 provirus via down-regulation of histone deacetylase 4 (HDAC4). *Proc. Natl Acad. Sci. USA* 109(34), E2284–E2293 (2012).

36 Mannaerts I, Eysackers N, Onyema OO *et al.* Class II HDAC inhibition hampers hepatic stellate cell activation by induction of microRNA-29. *PLoS ONE* 8(1), e55786 (2013).

37 Spallotta F, Tardivo S, Nanni S *et al.* Detrimental effect of class-selective histone deacetylase inhibitors during tissue regeneration following hindlimb ischemia. *J. Biol. Chem.* 288(32), 22915–22929 (2013).

38 Momose F, Naito T, Yano K, Sugimoto S, Morikawa Y, Nagata K. Identification of Hsp90 as a stimulatory host factor involved in influenza virus RNA synthesis. *J. Biol. Chem.* 277(47), 45306–45314 (2002).

• **Interesting research article about the role of Hsp90 during influenza virus replication cycle.**

39 Naito T, Momose F, Kawaguchi A, Nagata K. Involvement of Hsp90 in assembly and nuclear import of influenza virus RNA polymerase subunits. *J. Virol.* 81(3), 1339–1349 (2007).

• **Interesting research article about the role of Hsp90 during influenza virus replication cycle.**

40 Amatore D, Sgarbanti R, Aquilano K *et al.* Influenza virus replication in lung epithelial cells depends on redox-sensitive pathways activated by NOX4-derived ROS. *Cell. Microbiol.* 17(1), 131–145 (2015).

41 Mahay BWJ. *Virology: A Practical Approach.* IRL Press, Oxford, UK, 119–150 (1991).

42 Lahm A, Paolini C, Pallaoro M *et al.* Unraveling the hidden catalytic activity of vertebrate class IIa histone deacetylases. *Proc. Natl Acad. Sci. USA* 104, 17335–17340 (2007).

43 Bradner JE, West N, Grachan ML *et al.* Chemical phylogenetics of histone deacetylases. *Nat. Chem. Biol.* 6, 238–243 (2010).

44 Mosmann T. Rapid colorimetric assay for cellular growth and survival: application to proliferation and cytotoxicity assays. *J. Immunol. Methods* 65(1–2), 55–63 (1983).

45 Piacentini R, Li Puma DD, Ripoli C *et al.* Herpes simplex virus type-1 infection induces synaptic dysfunction in cultured cortical neurons via GSK-3 activation and intraneuronal amyloid-β protein accumulation. *Sci. Rep.* 5, 15444 (2015).

46 Valente S, Conte M, Tardugno M *et al.* Pyrrole-based hydroxamates and 2-aminoanilides: histone deacetylase inhibition and cellular activities. *ChemMedChem* 4(9), 1411–1415 (2009).

•• **Very interesting research article regarding the inhibitory deacetylase activity of a new class II-selective histone deacetylase inhibitors.**

47 Sinisterra JV, Moulounguí Z, Delmas M, Gaset A. Barium hydroxide as catalyst in organic reactions. V. Application in the Horner reaction under solid-liquid phase-transfer conditions. *Synthesis* 1985(12), 1097–1100 (1985).

• **An interesting research article regarding a application of a barium hydroxide catalyst for the Horner reaction.**

48 Suzuki T, Ando T, Tsuchiya K *et al.* Synthesis and histone deacetylase inhibitory activity of new benzamide derivatives. *J. Med. Chem.* 42(15), 3001–3003 (1999).

•• **An interesting research article regarding the synthesis and the inhibitory deacetylase activity of histone deacetylase inhibitors.**

49 Butler KV, Kalin J, Brochier C, Vistoli G, Langley B, Kozikowski AP. Rational design and simple chemistry yield a superior, neuroprotective HDAC6 inhibitor, tubastatin A. *J. Am. Chem. Soc.* 132(31), 10842–10846 (2010).

50 Tai VWF, Verner E, Balasubramanian S, Lee CS, Buggy JJ. WO 2007109178 A3 (2007).

51 Khan N, Jeffers M, Kumar S *et al.* Determination of the class and isoform selectivity of small-molecule histone deacetylase inhibitors. *Biochem. J.* 409(2), 581–589 (2008).

52 Spallotta F, Rosati J, Straino S *et al.* Nitric oxide determines mesodermic differentiation of mouse embryonic stem cells by activating class IIa histone deacetylases: potential therapeutic implications in a mouse model of hindlimb ischemia. *Stem. Cells* 28(3), 431–442 (2010).

53 Hildmann C, Wegener D, Riester D *et al.* Substrate and inhibitor specificity of class 1 and class 2 histone deacetylases. *J. Biotechnol.* 124(1), 258–270 (2006).

54 Balasubramanian S, Ramos J, Luo W, Sirisawad M, Verner E, Buggy JJ. A novel histone deacetylase 8 (HDAC8)-specific inhibitor PCI-34051 induces apoptosis in T-cell lymphomas. *Leukemia* 22(5), 1026–1034 (2008).

55 Scroggins BT, Robzyk K, Wang D *et al.* An acetylation site in the middle domain of Hsp90 regulates chaperone function. *Mol. Cell* 25(1), 151–159 (2007).

• **An interesting research article regarding the acetylation site of Hsp90 by HDAC6 and its role in Hsp90 chaperone function.**

56 Bali P, Pranpat M, Bradner J *et al.* Inhibition of histone deacetylase 6 acetylates and disrupts the chaperone function of heat shock protein 90: a novel basis for antileukemia activity of histone deacetylase inhibitors. *J. Biol. Chem.* 280(29), 26729–26734 (2005a).

57 Kovacs JJ, Murphy PJ, Gaillard S *et al.* HDAC6 regulates Hsp90 acetylation and chaperone-dependent activation of glucocorticoid receptor. *Mol. Cell* 18, 601–607 (2005).